Bifurcations and Chaos in the MAPK Signaling Cascade

Martin Zumsande[a,*], Thilo Gross[a]

[a]*Max Planck Institute for the Physics of Complex Systems, Nöthnitzer Str. 38, 01187 Dresden, Germany.*

Abstract

The mitogen-activated protein kinase (MAPK) cascade is an important signaling cascade in eukaryotes. We use the approach of generalized modeling to analyze the dynamics of the MAPK cascade and identify key mechanisms of instability. Furthermore, we report sustained multi-mode oscillations and potentially chaotic behavior caused by a sequestration-based feedback mechanism. Finally, we investigate the interplay between sequestration and external feedback loops. Our analysis thereby confirms, extends and generalizes previous results obtained by conventional modeling and points out the diversity of dynamics that sequestration can bring about.

Keywords: Modelling, Signalling networks, Phosphorylation, Bistability

1. Introduction

The mitogen-activated protein kinase (MAPK) pathway is involved in the regulation of numerous cell functions, among them proliferation, apoptosis, differentiation and cell motility (Seger and Krebs, 1995; Chang and Karin, 2001; Johnson and Lapadat, 2002). Moreover, in many types of cancer, dysfunctions in the MAPK pathway have been detected (Downward, 2003; Roberts and Der, 2007). Therefore, a heightened understanding of the pathway may potentially lead to the discovery of new drug targets for cancer treatment.

While there are several variants of MAPK cascades depending on organism and signal type, the topological motif shown in Fig. 1 is conserved in MAPK pathways throughout all eukaryotic cells (Seger and Krebs, 1995). In the figure, we show a prominent example of a MAPK cascade, the growth-factor induced Ras-Raf-MEK-ERK cascade. When a cell is exposed to certain growth factors, a series of intermediate reactions is triggered that ultimately lead to the activation of the enzyme Ras, which itself phosphorylates Raf, a protein also called MAPKKK (MAP-Kinase-Kinase-Kinase). In its activated state, Raf can phosphorylate the protein MEK (MAPKK) at two different sites. The double-phosphorylated MEK can then act as an enzyme in the double phosphorylation of ERK (MAPK), which activates several transcription factors and downstream kinases in its phosphorylated state. Metabolic Control Analysis (MCA) suggests that these reactions downstream from Ras, the actual cascade, are most important for the dynamics (Hornberg et al., 2005).

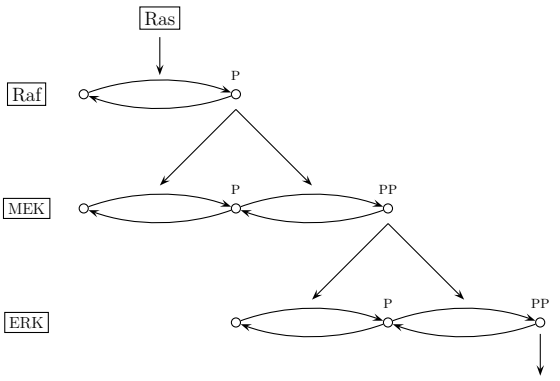

Figure 1: Diagrammatic representation of the MAPK signaling cascade. The pathway consists of three layers, a single phosphorylation loop at the top layer and two double-phosphorylation loops at the other layers. Phosphorylated forms are indicated by P's in the figure. The fully phosphorylated product in each level acts as a kinase phosphorylating the proteins on the level below.

The first mathematical model of the MAPK cascade was formulated by Huang and Ferrell (Huang and Ferrell, 1996), showing that the system can act as an ultrasensitive switch. Later, it was found that adding explicite negative feedback leads to oscillations (Kholodenko, 2000) and that the combination of double phos-

*Corresponding author

Email address: zumsande@mpipks-dresden.mpg.de (Martin Zumsande)

phorylation and enzyme sequestration introduces an implicit feedback leading to bistability (Markevich et al., 2004) and oscillations (Qiao et al., 2007). Most investigations adopted the ranges of model parameters (concentrations and rate constants) from (Huang and Ferrell, 1996), based on measurements in *Xenopus* oocyte extracts. However, little is known about the possible parameter ranges in which eukaryotic cells can operate in different species and at different developmental stages. It has been argued before that the complicated structure of a three-layered double-phosphorylation cascade could have evolved as a result of an optimization of the response time to signals (Frey et al., 2008). However, there may also be adaptive advantages for the realization chosen by nature that are based on other dynamical properties of the underlying models.

In this paper we apply the approach of generalized modeling (Gross and Feudel, 2006; Steuer et al., 2006; Gross et al., 2009) to the MAPK cascade. The main advantage of this approach is that it avoids simulation, which is numerically demanding and can be unreliable for some systems. While generalized models reveal only certain types of information, this information is gained very efficiently, allowing us to explore a large parameter space.

Our analysis identifies the key parameters that govern the stability of stationary states of the MAPK cascade. We then analyze the transitions in which the stability is lost. This reveals regions of oscillatory behavior and provides evidence for bistability, generalizing previous results. Then we apply the generalized analysis to identify a parameter region in which complex dynamics can be observed. Finally, we investigate the effect of external feedback mechanisms on the dynamics of the cascade.

2. Formulation of the model

2.1. Generalized modeling

The example of the MAPK signaling pathway presents a typical challenge: While the structure of the underlying network of protein interactions is relatively well known, the functioning of the system is closely linked to its dynamics and therefore difficult to observe in experiments. Conventional modeling approaches aiming at exploring the dynamics of the system are forced to restrict every process to a specific rate law. It is therefore often not clear whether the observed dynamics represents robust behavior of the system or arises only because of the specific choice of functional forms. Moreover, the exploration of the long-term behavior of conventional models by direct simulation is numerically inefficient. Computational restraints therefore impose strong limits on the size of the parameter space that can be explored.

The approach of generalized modeling is based on the insight that certain information can be extracted more efficiently by considering the whole class of plausible models (Gross and Feudel, 2006; Steuer et al., 2006; Gross et al., 2009). Instead of parameterizing the specific rate laws in the model, we directly parameterize the Jacobian matrix, governing the dynamics close to all possible steady states in all models that are consistent with the observed interaction network. Only subsequently is the class of models under consideration narrowed down by fixing certain parameters of the generalized model.

Before we focus specifically on the MAPK cascade, let us introduce the approach of generalized modeling as such. For this purpose consider a given network of biochemical interactions regulating the concentrations of a number of proteins. If the concentrations are sufficiently high to neglect stochastic effects, the dynamics of the system can be captured by a system of differential equations of the form

$$\frac{\mathrm{d}}{\mathrm{dt}}\mathbf{S}(t) = \mathbf{N}\boldsymbol{f}(\mathbf{S}), \tag{1}$$

where $\mathbf{S}$ is a vector of protein concentrations, $\mathbf{N}$ is the stoichiometric matrix and $\boldsymbol{f}$ is a flux vector depending on the S_i.

Assuming that a positive, but not necessarily stable, steady state $\mathbf{S}^*$ exists, this equation can be normalized with respect to the steady state concentrations and written in the form

$$\frac{\mathrm{d}}{\mathrm{dt}}\mathbf{x} = \mathbf{\Lambda}\boldsymbol{\mu}(\mathbf{x}) \tag{2}$$

with $x_i = S_i/S_i^*$, $\Lambda_{ij} = N_{ij}f_j(\mathbf{S}^*)/\mathbf{S}_\mathbf{i}^*$ and $\mu_i(\mathbf{x}) = \mathbf{f_i}(\mathbf{S})/\mathbf{f_i}(\mathbf{S}^*)$.

The local dynamics close to the steady state $\mathbf{S}^*$ is governed by the corresponding Jacobian matrix defined as $J_{ij} = \partial S_i(t)/\partial S_j\big|_{\mathbf{S}^*}$. Since $\mathbf{\Lambda}$ does not depend on $\mathbf{x}$ the Jacobian of our system can be written as

$$\mathbf{J} = \mathbf{\Lambda}\boldsymbol{\theta}_\mathbf{x}^{\boldsymbol{\mu}} \tag{3}$$

with

$$\boldsymbol{\theta}_{x_i}^{\mu_j} = \left.\frac{\partial \mu_j(\mathbf{x})}{\partial x_i}\right|_{\mathbf{S}^*}. \tag{4}$$

The steady state under consideration is stable if all eigenvalues of the Jacobian have negative real parts and unstable if at least one eigenvalue has a positive real part.

Changing the parameters can bring about a loss of stability when it causes a single real eigenvalue or a complex conjugate pair of eigenvalues to cross the imaginary axis of the complex plane, acquiring a positive real part. The former case corresponds to a saddle-node bifurcation in which the number of steady states changes, while the latter corresponds to a Hopf bifurcation in which a limit cycle emerges.

The entries of $\mathbf{\Lambda}$ and $\boldsymbol{\theta}_x^{\boldsymbol{\mu}}$ constitute a complete parameterization for the entire range of possible Jacobians that are consistent with the underlying topology of biochemical interactions. Since we have not specified the right-hand-side of the equations of motion, Eq. 2, we cannot compute the steady states of the system with the chosen degree of generality. Therefore, also the entries of the Jacobian matrix, which depend on the steady state, remain unknown. However, the quantities appearing in the Jacobian are constants and can therefore be interpreted as unknown parameters with the same right as the parameters that are usually introduced in conventional modeling.

In general, the generalized parameters can be related to parameters appearing in conventional models (Van Voorn et al., 2008; Stiefs et al., 2009). Given a steady state from a conventional model, it is straightforward to compute the corresponding generalized parameters. Conversely, a single set of generalized parameters can be translated to a family of conventional models, exhibiting a corresponding steady state. While the difficulty of the latter depends on the functional forms that are assumed in the conventional model, it is no major obstacle in the models with mass action used in this paper.

The parameters identified by the generalized modeling procedure have an intuitive biological interpretation: The entries of $\mathbf{\Lambda}$ have the dimension of an inverse time and represent characteristic time scales of the model. They are therefore called scale parameters in generalized modeling. The entries of $\boldsymbol{\theta}_x^{\boldsymbol{\mu}}$ are logarithmic derivatives of the fluxes. The corresponding parameters are called exponent parameters in the context of generalized models and elasticities in the context of metabolic control theory (Fell, 1992). Note, for example that if one of the processes in the model is linear $f_i \sim S_j$ the corresponding exponent parameter is $\theta_{ij} = 1$, irrespective of the constant of proportionality. More generally, for any power-law relationship $f_i \sim {S_j}^p$ the corresponding parameter is the exponent $\theta_{ij} = p$. Even for functions that are not power laws, the exponent parameters can be interpreted as a measure of the local nonlinearity.

In the steady state under consideration all fluxes in the model have to balance $\mathbf{N}\boldsymbol{f}(\mathbf{S}^*) = \mathbf{0}$, which constitutes a constraint for the permissible values of scale parameters. To satisfy this constraint and reduce the number of free parameters it can be advantageous to use an alternative parameterization based on the *flux modes* of the model (Steuer et al., 2007). In this parameterization the scale parameters denote the strength of the independent flux modes that are consistent with the stationarity condition.

In summary, the generalized model provides a parameterization of the Jacobian in all steady states that can be found in a class of models defined by a given interaction topology. While the analysis of the Jacobian can only reveal certain types of information it does so with a high degree of robustness and numerical efficiency. Although numerical simulation of conventional models is useful to supplement insights gained from generalized modeling, the generalized model allows us to explore dynamics close to steady states without resorting to numerical simulation. The analysis of the Jacobian matrix benefits from the availability of highly efficient algorithms for the computation of eigenvalues. Therefore, in models of intermediate complexity, say less than 50 dynamical variables, several tens of billions parameter sets can be explored in reasonable computational time (Gross et al., 2009). By comparison, for the present model already the analysis of just tens of millions of parameter sets yields sound statistical results.

2.2. Model of the MAPK cascade

In our model of the MAPK cascade we use the following naming convention: The symbol ${S^i}_j$ is used to denote the concentrations of proteins and protein complexes which appear as substrates in the model. The superscript index i indicates the layer of the cascade in which the specific protein is involved, while the subscript index j enumerates all proteins in the respective layer. Note that, although we avoid the use of asterisks, in the following all symbols ${S^i}_j$ denote concentrations in the steady state.

The concentrations of the additional free kinases and phosphatases that do not appear as substrates themselves are labeled K^i_{R} and P^i_{R}, respectively. The total concentrations of the substrates, kinases and phosphatases in a given layer of the cascade are denoted ${S^i}_{\mathrm{T}}$, K^i_{T} and P^i_{T}. As these concentrations are conserved in the context of the model, they constitute constant external parameters. These naming conventions are illustrated in Fig. 2.

In the following we consider three different models describing subsystems of the MAPK cascade of different complexity. The first of these models contains only

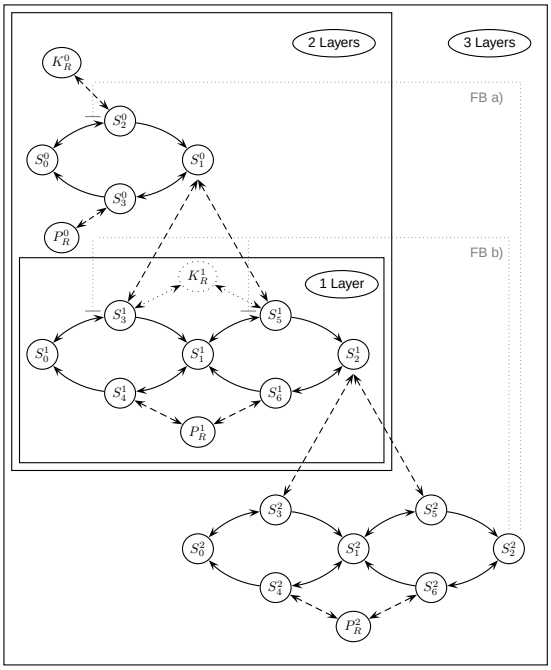

Figure 2: Schematic overview of the MAPK cascade. The solid arrows correspond to biochemical reactions while the dashed arrows denote the binding of an enzyme in the formation of an substrate-enzyme complex. The dotted kinase K_{R}^1 (1-layer model) is replaced by S_1^0 in the larger models. The three different subsystems that we analyzed separately are indicated by boxes. The gray dotted lines represent two types of feedback, which are only included in the model in Sec. 3.7.

a double phosphorylation step as it occurs in the second layer of the cascade whereas the first and third layer are neglected. The second model contains the first and the second layer of the cascade, but neglects the third. Finally, the third model contains all three layers. The scope of the different models is indicated by boxes in Fig. 2. The kinase that catalyzes the phosphorylation in the second layer is called K_{R}^1 in the first model in order to indicate that, in the scope of this model, it is not a substrate by itself. In the two larger models it is called S_1^0 as it appears as a substrate in the first layer.

For the dynamics of the cascade, enzyme sequestration is suspected to be of central importance (Blüthgen et al., 2006; Legewie et al., 2007; Qiao et al., 2007). Sequestration can affect the dynamics because an enzyme that is bound to a substrate cannot at the same time participate in other reactions, including its own dephosphorylation. Without external feedback, sequestration effects provide the only means by which the concentrations on the lower layers of the cascade can affect the dynamics on the layers above. To capture the sequestration effects explicitly we follow (Qiao et al., 2007) and break each phosphorylation step into two separate processes, for example

$$S_0^0 + K_{\mathrm{R}}^0 \underset{k_1}{\overset{k_0}{\rightleftharpoons}} S_2^0 \xrightarrow{k_2} S_1^0 + K_{\mathrm{R}}^0, \tag{5}$$

The first step represents the reversible binding of the kinase K to the unphosphorylated substrate S_0^0, while the second step represents the action of the kinase resulting in the release of the phosphorylated substrate S_1^0. Other approaches such as Michaelis-Menten based enzyme kinetics can miss sequestration effects. Although a sequestration-based approximation scheme has been proposed recently (Ventura et al., 2008), the efficiency of generalized modeling does not rely on the number of reactions or variables being small. We therefore avoid this approximation and represent the complexes explicitly in the model.

Assuming that the concentrations of proteins are sufficiently high to be considered as continuous variables, we capture the dynamics of the cascade by a system of coupled ODEs. For the phosphorylation step in the top layer of the cascade we obtain

$$\begin{aligned}
\frac{\mathrm{d}}{\mathrm{dt}} S_0^0 &= -f_1(S_0^0, K_{\mathrm{R}}^0) + f_2(S_2^0) \\
\frac{\mathrm{d}}{\mathrm{dt}} S_2^0 &= f_1(S_0^0, K_{\mathrm{R}}^0) - f_2(S_2^0) \\
\frac{\mathrm{d}}{\mathrm{dt}} S_1^0 &= f_3(S_2^0)
\end{aligned} \tag{6}$$

where f_1, f_2, and f_3 are general functions, which are not yet restricted to specific functional forms.

Starting from the set of differential equations, the Jacobian of the generalized model is obtained by following the steps outlined in the previous section. While we omit this derivation here the resulting equations are shown in the supplementary material. Also, the complete derivation of the generalized model for the one-layer model is shown for the purpose of illustration in the appendix.

As the model explicitly describes the complexes formed by enzymes with their substrates, it is reasonable to assume that the remaining processes are governed by mass action. We therefore utilize the ability of generalized models to deal with general functions only when considering the effect of external feedbacks, while the ability to explore large parameter spaces is used throughout the whole study. With this choice our model corresponds directly to the conventional models considered in (Huang and Ferrell, 1996; Qiao et al., 2007).

Note that even if it is assumed that the processes are linear, the system of equations is nonlinear as it includes bilinear terms. Using mass conservation to express the concentrations of certain proteins as a function of others (see appendix) changes some of the bilinear terms into explicit quadratic nonlinearities.

3. Investigation of the dynamics

3.1. Stability analysis of the single-layer model

Following Qiao et al. (2007), we started by investigating the second layer of the cascade in isolation. This comparably simple system is still analytically tractable and has been investigated in earlier work (Markevich et al., 2004; Ortega et al., 2006).

To identify the parameters that have a strong impact on the stability of steady states we created a large ensemble of 10^6 parameter sets where the parameters in each set were generated as follows: We first drew the concentrations of S_3^1, S_5^1 and K_R^1 from a uniform distribution. These concentrations were then normalized such that $K_T^1 = S_3^1 + S_5^1 + K_R^1 = 1$. Then, S_4^1, S_6^1 and P_R^1 were drawn randomly and normalized such that $P_T^1 = S_4^1 + S_6^1 + P_R^1 = 1$. To ensure that sequestration effects can have an impact on the dynamics we set the total concentration S_T^1 of the substrate to 10, so that there is considerably more substrate than kinases and phosphatases. A fraction of the substrate is already bound in the complexes S_3^1, S_5^1, S_4^1, and S_6^1. We distribute the remainder $r = S_T^1 - S_3^1 - S_5^1 - S_4^1 - S_6^1$ by drawing random concentrations for S_0^1, S_1^1, and S_2^1 and normalizing so that $S_0^1 + S_1^1 + S_2^1 = r$. Finally we drew the strength of all flux modes in the model randomly from a uniform distribution.

In order to assess the impact of the individual parameters on stability we computed the stability of the steady state in each sample parameter set. Stable steady states were assigned the stability value 1 whereas unstable states were assigned the stability value 0. For each parameter we then computed the Pearson correlation coefficient of the focal parameter with the stability value across the whole ensemble.

For the single layer the correlation coefficients are shown in Fig. 3A. The concentrations of the unbound kinase K_R^1 and phosphatase P_R^1 show a correlation coefficient of 0.21 with stability. Consequently the system is likely to be stable if these concentrations are high and unstable if they are low. This shows that instability occurs most likely if a large fraction of the kinase and phosphatase is sequestered in complexes. Particularly, the complexes S_3^1 and S_6^1, which are involved in the production of the single-phosphorylated S_1^1 are negatively correlated with stability, showing that a high concentration of these complexes has a strong destabilizing effect. By contrast, the complexes S_4^1 and S_5^1 which appear in reactions decreasing S_1^1 are positively correlated with stability.

More detailed insights in the effect of important parameters can be gained by plotting the fraction p of randomly drawn steady states that are stable. For this purpose we generated another ensemble of 10^7 parameter sets as described above. Figure 4 shows p as a function of selected combinations of two parameter values. In Fig. 4A, p is shown as a function of the free enzyme concentrations K_R^1 and P_R^1. The figure reveals that low concentrations of either K_R^1 and P_R^1 promote instability. This confirms that sequestration plays a role in the destabilization of steady states. The dependence of p on the parameters S_3^1 and S_6^1, which were found to have a strongly destabilizing impact, is plotted in Fig. 4B. The figure shows that the fraction of stable states changes very sharply as a threshold is crossed. By comparison, even if the stabilizing parameters S_4^1 and S_5^1 are very low p only drops to 0.5 (Fig. 4C). The comparison confirms the lesser impact of the two stabilizing parameters, already seen in the correlation analysis. This conclusion is further supported by the direct comparison of the destabilizing parameter S_3^1 with the stabilizing parameter S_4^1 (Fig. 4D). In summary we conclude that the main source of instability in the single-layer system lies in high concentrations of the complexes S_3^1 and S_6^1.

3.2. Mechanisms of instability

To understand the mechanism leading to instability in more detail we consider the eigenvectors of the system's Jacobian. In an unstable steady state the eigenvector corresponding to largest (positive) eigenvalue represents the direction of perturbation in the state space of the system that grows most rapidly in time. Therefore, the eigenvector also marks the direction in which the system leaves the steady state after destabilization occurs. We computed the typical direction of escape from the unstable steady state by averaging over the eigenvectors of the largest eigenvalue in 10^6 unstable parameter sets generated randomly. The components of this averaged direction of escape are shown symbolically in Fig. 5. The figure illustrates that the instability causes the proteins to shift into either one of the phosphorylation cycles, while depleting the other.

The nature of the instability described above can be linked to the destabilizing effect of S_3^1 and S_6^1. If there is a large concentration of S_3^1 (or, S_6^1) then the kinase (phosphatase) is not available for the formation of the

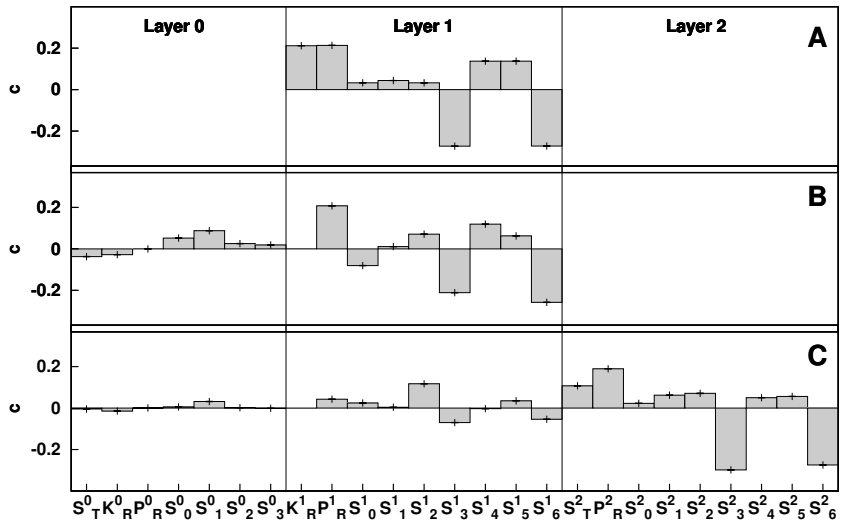

Figure 3: Correlations of parameters with stability. We consider three different subsystems of the cascade, a single layer (A), two connected layers (B) and three layers (C). The bars show the correlation of a given parameter with the stability of the steady states in a large ensemble of randomly generated parameter sets. The statistical errors, which are determined by bootstrap resampling, are on the order of the line width. The plots show a conserved pattern of correlations and indicate the parameters that are important for stability.

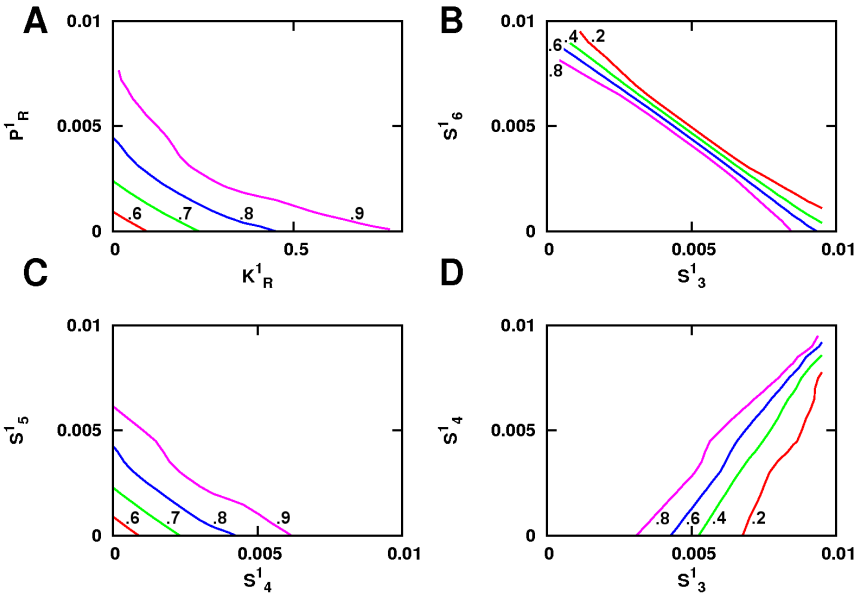

Figure 4: Connection between steady-state concentrations and stability. Contour lines computed from 10^7 random parameter sets show the fraction of stable systems depending on the two concentrations. The top left panel shows that instability is promoted by low concentrations of free kinase and phosphatase, highlighting the importance of sequestration effects. The model parameters with the strongest impact on stability are the concentrations of substrates S^1_3 and S^1_6 (top right).

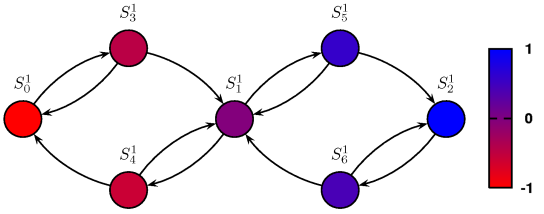

Figure 5: Instability in a single layer of the cascade. The components of the eigenvector corresponding to the largest eigenvalue of the Jacobian are analyzed. For each dynamic variable, the color indicates the averaged value of the corresponding entry of the eigenvector. All eigenvectors were normalized so that $S_5^1 = 1$ before taking the average over 10^6 samples. The diagram shows that the systems leaves the region of a typical unstable state by accumulating mass in either one of the two phosphorylation cycles, while depleting the other.

complex S_5^1 (S_4^1). This implies the primary reaction involving S_1^1 as a substrate is binding in the complex S_4^1 (S_5^1). This leads to accumulation in the left (right) phosphorylation loop and consequently increases S_3^1 (S_6^1) further. Thus a positive feedback loop is formed that causes the instability.

3.3. Relation to bistability

Unstable steady states are often located on a separatrix that divides the basins of attraction of different attractors. Also in the MAPK cascade previous works have shown that a single layer of the cascade can support bistable dynamics (Markevich et al., 2004; Qiao et al., 2007), in which the system can approach either one of two stable steady states. To confirm that the unstable steady states observed in the generalized model mark the separatrix between two stable steady states, we simulated the dynamics of the conventional model used in (Qiao et al., 2007) using a stiff numerical integrator based on the modified extended backward differentiation formula (MEBDF) (Hairer and Wanner, 1991). We randomly selected 100 starting points corresponding to unstable states computed in the generalized model. For all of these points we found that multiple trajectories starting close to the steady state eventually converged to two different final states. An example time series is shown in the supplementary material. This result suggests that, in a class of reasonable conventional models of the second layer of the MAPK cascade, the long-term dynamics is bistable whenever we find an unstable steady state in the generalized model.

3.4. Stability in larger models

As a next step we considered the stability of two larger subsystems of the cascade. We proceeded analogously to the investigation of the single-layer model by first generating a large ensemble of randomly drawn parameter sets and then correlating the stability of the corresponding steady states with the parameter values.

In the investigation of the larger models, describing two and three layers of the cascade, we slightly altered our procedure for generating random parameter sets in order to generate sets that are close to empirical observations, using data from Huang and Ferrell (1996). The details of this procedure are explained in the appendix.

The results of a correlation analysis are shown in Fig. 3B,C. Figure 3B shows the stability correlations in our second model, which consists of the first and second layer of the cascade. While there are now more parameters than in model 1 (Fig. 3A), the additional parameters, describing the top layer of the cascade have a weaker impact on the stability of steady states, as evidenced by the low values of the corresponding correlation coefficients. Note furthermore that the pattern of correlation coefficients in the second model is very similar to that found in the first model. In particular, there is a repeated motif of strong positive correlations in P_R^1, S_4^1, and S_5^1 and strong negative correlations in S_3^1 and S_6^1.

In the third model, consisting of all three layers of the cascade, the pattern of correlations observed above reappears twice. As shown in Fig. 3C, the correlation coefficients corresponding to both the first and second layer of the cascade are now quite small, indicating a much reduced impact on the dynamics. Nevertheless the pattern of correlations is still visible in the second layer. More importantly, the pattern reappears in a stronger form in the third layer. Thus, the correlation analysis shows that the basic mechanism of instability, the positive feedback induced by sequestration of substrates into the complexes S_3 and S_6, remains the same in all three models.

3.5. Oscillatory instabilities

In the next step, we focused on the dynamics that can be observed in the two and three layer systems after the stability of a steady state has be lost. For this purpose we searched for the bifurcation points, marking a change in the stability of a steady state. Since the probability of finding a bifurcation point by random sampling is of measure zero, we generated a ensemble of 10^7 random parameter sets as described above, but selected only those parameter sets in which the real part of the leading eigenvalue of the Jacobian in the steady state was in the range [0,0.01], indicating proximity to a bifurcation point. Those parameter sets were then settled to the bifurcation manifold by a Newton fixed-point algorithm (Kelley, 2003).

In the single-layer model this procedure yields only bifurcation points of saddle-node type, which in this model mark the onset of bistability. The absence of Hopf bifurcations, which typically correspond to the onset of oscillatory dynamics, supports the previously observed absence of oscillations in the single-layer model. In the two and three-layer models we find both Hopf and saddle-node bifurcations, which shows that both bistability and oscillations are generically possible in these models.

Further insights can be gained by investigating the dynamics close to unstable steady states. For all unstable steady states found in 10^7 samples we checked whether the leading eigenvalue, which governs the departure from the steady state, is real or complex valued. In the one-layer model, we found no unstable steady states with complex leading eigenvalues, providing further evidence for the absence of oscillatory dynamics. By contrast, leading complex eigenvalues are found in 4% of the unstable steady states of the two-layer system and in 34% of the unstable steady states of the three-layer system. This suggests that oscillatory dynamics appear more prominently in the three-layer cascade.

3.6. Complex global dynamics

Since we saw that oscillatory dynamics is absent in the one-layer system, but appears when a second layer is added, one can ask whether even more complex dynamics such as quasiperiodicity or chaos can occur in the three-layer system. Generalized modeling, being essentially based on a local analysis, cannot detect such global dynamics directly. However, generalized models can be used to search for local bifurcations of higher codimension that can serve as proxies for complex dynamics.

In order to find a bifurcation of codimension two, one must adjust two parameters of the system simultaneously to their exact bifurcation values. Therefore, codimension-2 bifurcations are almost never observed directly in experiments and have, for the lack of examples, received relatively little attention in the mathematical literature (Guckenheimer and Holmes, 1997)(p. 420). Nevertheless the identification of codimension-2 bifurcations can reveal many insights in the dynamics of a system because of their role of organizing centers for different types of dynamics.

An example of a codimension-2 bifurcation is shown in Fig. 6 in a three-parameter bifurcation diagram, which was created by a triangulation procedure described in (Stiefs et al., 2008). The parameters are given in Table S1 in the supplementary material. In the three-dimensional parameter space a surface of Hopf bifurcation points (light surface) and a surface of saddle-node bifurcation points (dark surface) intersect. On the intersection line of the surfaces the Jacobian has both a single zero eigenvalue and a purely imaginary eigenvalue pair, marking the points on the intersection line as codimension-2 Gavrilov-Guckenheimer bifurcation points. It is well known from normal form analysis that close to this type of bifurcation quasiperiodic dynamics should generally occur (Kuznetsov, 1995)(p. 345). Another example of a codimension-2 bifurcation is the double-Hopf bifurcation, which is characterized by the presence of two purely imaginary eigenvalue pairs. This bifurcation generically involves the creation of chaotic and quasiperiodic regions (Kuznetsov, 1995)(p. 369).

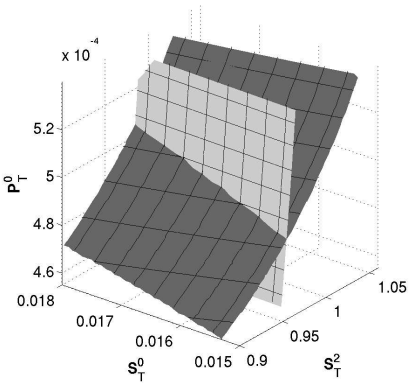

Figure 6: Three-parameter bifurcation diagram of a codimension-2 Gavrilov-Guckenheimer bifurcation. The codimension-2 bifurcation is formed at the intersection line of a Hopf bifurcation (light gray) with a saddle-node bifurcation (dark gray). Bifurcations of higher codimension such as Gavrilov-Guckenheimer and double Hopf bifurcations can serve as proxies that indicate parameter regions in which complex dynamics can potentially be observed. See the supplementary material for additional parameters.

While the presence of Gavrilov-Guckenheimer and double Hopf bifurcations cannot guarantee complex long-term behavior, they serve as proxies indicating parameter regions in which such complex dynamics is likely. We therefore used the generalized model to search specifically for these bifurcations. Explicit numerical simulation of the conventional model was then used to explore the dynamics close to these bifurcation points. In this way the greater efficiency of generalized models is combined with the higher predictive power of conventional models. In the model of the MAPK cascade we observed interesting dynamics only close to double-Hopf bifurcations, which appear exclusively in the three-layer system. A two-parameter bifurcation diagram of a double-Hopf bifurcation and two ex-

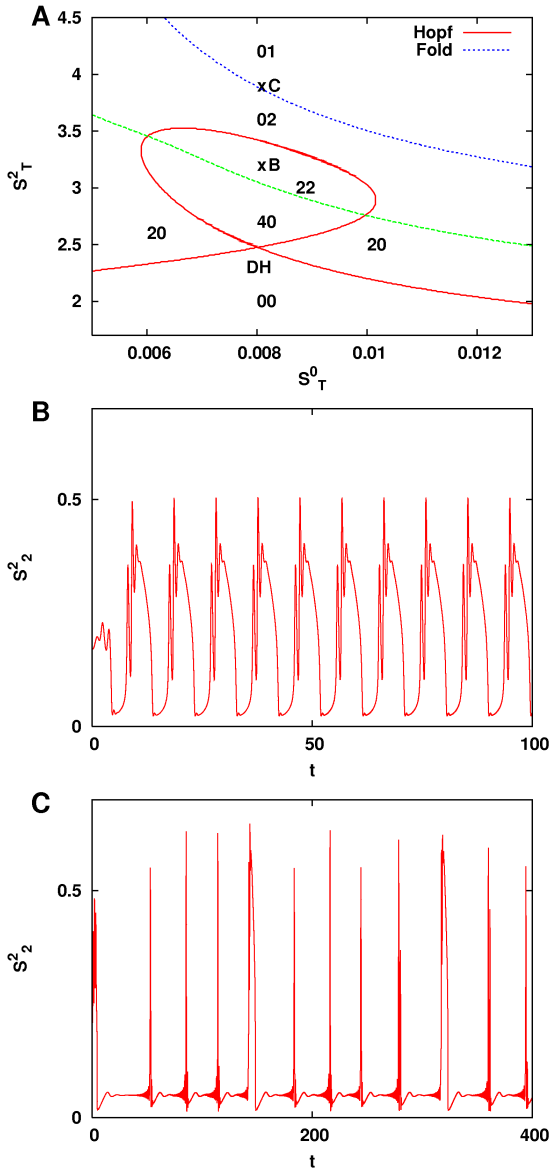

Figure 7: Complex dynamics close to a double-Hopf bifurcation. **A**: Two-dimensional bifurcation diagram with a double Hopf bifurcation. Parameters are S^0_T and S^2_T. Hopf bifurcations are drawn in red, saddle-node bifurcations in blue. At the green line (AP), a Hopf pair loses its imaginary part, leading to two distinct real eigenvalues. The numbers denote the number of complex and real eigenvalues with a positive real part, in this order. This means that the stable region is marked by 00. The points B and C at which we show numerical integration results are drawn in. **B** and **C**: Complex oscillations and chaos close to the double-Hopf bifurcation.

ample time series from different regions are shown in Fig. 7. The corresponding parameters are listed in Table S1 and Table S2 in the supplementary material. Both timeseries show evidence of complex mixed-mode oscillations. Moreover the spike-like time-series shown in Fig. 7C exhibits an irregularity that is indicative of Šilnikov chaos. Similar dynamics were also observed at multiple points in the neighborhood (not shown). We are therefore confident that the system shows chaotic long-term behavior in a finite parameter region. However, to confirm the chaotic nature of the dynamics and to determine the parameter ranges in which they occur will require more extensive numerical investigations, including the computation of Lyapunov exponents, which exceed the scope of this paper.

3.7. Explicit Feedback

In addition to the sequestration-mediated negative feedback inherent in the cascade, we also considered the implications of adding explicit feedback loops. While the structure of the MAPK cascade is widely conserved throughout eukaryotic cells, this is not necessarily true for the types of feedback that may depend on species and tissue (Kolch et al., 2005). Here we consider two types of mechanisms: a) In fibroblasts, inhibitory phosphorylation of SOS, a protein upstream from Ras (K^0_R), by ERK (S^2_2) effectively inhibits the formation of the Ras-Raf complex (S^0_2) (Langlois et al., 1995; Kholodenko, 2000). b) In COS1-cells, activated ERK (S^2_2) feeds back to MEK (S^1_0) during cell adhesion by phosphorylating it at the site T292, which inhibits phosphorylation by PAK at the adjacent site S298. The suppressed phosphorylation facilitates the formation ERK-Raf complexes (S^1_3,S^1_5) (Eblen et al., 2004), resulting in a negative feedback of S^2_2 on S^1_0.

As it is widely believed that the MAPK cascade is utilized mainly as an ultrasensitive switch, we ask whether the feedback loops act to suppress other dynamics, such as oscillations. We therefore investigated whether the oscillatory regime is reduced by introducing feedback in the system. To study this question in conventional models is not trivial for two reasons: First, in a conventional model the effect of the feedback has to be restricted to a specific functional form, which can in practice be difficult to derive. Second, and perhaps more importantly, to study the effect of feedbacks in isolation in conventional models is not trivial. The question is typically how the stability of a given steady state observed in nature depends on the nonlinearity of the feedback. However, if feedback parameters in conventional models are changed one generally observes the combined effect of both the altered nonlinearity and the corresponding shift in the steady state. Both of these difficulties are easily avoided in generalized models as they are designed to deal with unknown functions and parameterize the po-

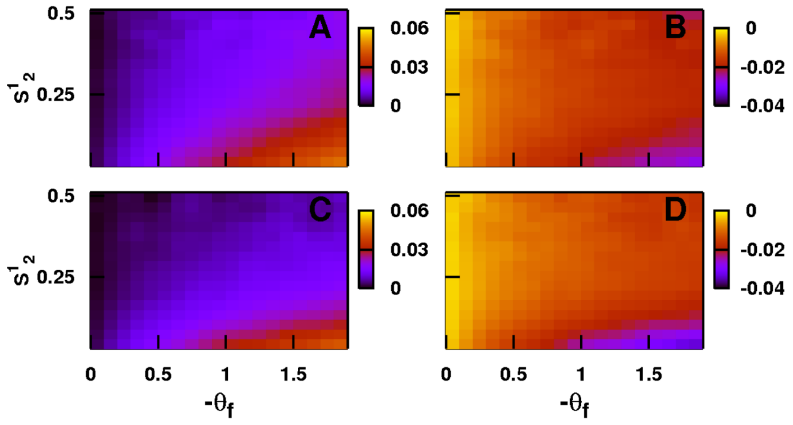

Figure 8: The effect of external feedback. Color-coded is the change in relative abundance of unstable stationary states as feedback is switched on. This change is shown separately for unstable states with leading complex eigenvalues (left) and leading real eigenvalues (right). The top row corresponds to feedback to the first layer (type a) while the bottom row corresponds to feedback to the second layer (type b). In both cases stronger feedback (large values of θ) means that more unstable steady states with a complex and less states with a real leading eigenvalue occur. This suggests that the feedbacks promote rather than inhibit oscillatory dynamics.

sition of the steady state independently from the nonlinearities in the system.

We studied the effect of the feedback of type a) and b) by adding an inhibitory link from the final product of the cascade, S_2^2, back to the phosphorylation steps in the first (a) and second (b) layer, respectively. In our model inhibitory feedback implies that the first derivative of the feedback function is negative. The effect of the feedback can therefore be modeled by introducing $\theta_f = \theta^{\mu_1}_{S_2^2} < 0$ (feedback a) and $\theta_f = \theta^{\mu_7}_{S_2^2} = \theta^{\mu_{13}}_{S_2^2} < 0$ (feedback b). In order to determine the effect of the feedback we generated an ensemble consisting of 10^7 parameter sets for each of the two feedback mechanisms. The parameter sets were drawn randomly, as described above, except for the additional feedback parameter θ_f, which were drawn randomly from a uniform distribution in the interval $[-2, 0]$. This range is for instance consistent with inhibition modeled by a Hill function with exponent two. For each parameter set, we then computed the spectrum of the Jacobian with and without feedback. While the stability of steady states corresponding to individual data sets changes when the feedback is switched on, the net effect on stability on the whole ensemble is small for both types of feedback (not shown). A stronger effect of the feedback becomes apparent if one considers the dynamics subsequent to the loss of stability. Figure 8 shows the change in the number of unstable states in which the leading eigenvalue of the Jacobian is complex or real, respectively. For both feedback mechanisms we observe that as the feedback parameter increases the number of unstable steady states with complex leading eigenvalues increases, while the number of unstable steady states with real leading eigenvalues decreases. Although the observation of an unstable steady state with complex leading eigenvalues does not imply that the long-term dynamics of the system is oscillatory, the increase of such states over a wide parameter range strongly suggests that also oscillatory long-term dynamics is promoted rather than suppressed by the two feedback loops under consideration.

4. Discussion

In this paper we used generalized modeling to analyze the dynamics of a class of models of different subsystems describing the MAPK cascade. By a correlation analysis, building on tens of millions of parameter sets, we determined the impact of the individual model parameters on the stability of the steady states. This analysis confirmed that sequestration of enzymes has a strong impact on the dynamics of the cascade. In particular, we showed that instability is likely if large portions of the kinase and phosphatase acting on the lowest level of the cascade are sequestered into complexes (S_3^2 and S_6^2 in our notation). In this case a positive feedback loop is formed that destabilizes stationary states.

In a second step we used bifurcation analysis, spectral analysis of unstable states, and explicit simulation to investigate the dynamics subsequent to the loss of stability. In a subsystem, consisting of only one layer of the cascade, bifurcation analysis of the generalized model revealed that steady states lose their stability only in saddle-node bifurcations. By contrast, in the two- and three-layer subsystems Hopf bifurcations as well as saddle-node bifurcations occur. In the present model it was confirmed by numerical simulations that the saddle-node bifurcations mark the onset of bistability, while the Hopf bifurcations mark the onset of oscillations. Our results are therefore in agreement with earlier work (Qiao et al., 2007) showing that, without external feedback, at least two layers of the cascade are required to observe oscillatory dynamics, while bistability already occurs in a single layer of the cascade.

Using a combination of generalized and conventional modeling we then identified a parameter region in which complex and potentially chaotic mixed-mode oscillations occur. To determine the exact nature of these oscillations and the parameter ranges in which they can be observed is a promising question for future studies, but will probably require more extensive numerical simulations and the computation of Lyapunov exponents.

Finally, we have investigated the impact of two known feedback loops acting on the MAPK cascade. Our analysis indicates that, under general conditions, the effect of these loops is to reduce bistability and promote oscillatory dynamics in the cascade.

Sustained oscillations in cells can be generated by several different mechanisms (Tyson et al., 2003). The most prominent cause of oscillations is negative feedback, sometimes in connection with a time delay. Explicit negative feedback led to sustained oscillations in various models of the MAPK cascade (Kholodenko, 2000; Shankaran et al., 2009) and indeed enlarged the oscillatory parameter regime in our model, too. However, negative feedback cannot explain the oscillations without explicit feedback, which must therefore rely on a different mechanism. It is known that in a system with positive feedback that exhibits bistability, a slow process can cause the system to jump between the two stable states. As a result, relaxation oscillations occur that usually have a pulselike shape (Kholodenko, 2006). Indeed, it was found that in the MAPK cascade, the second layer is in the regime of bistability when the whole system oscillates (Qiao et al., 2007). The bistable double phosphorylation loop is controlled by a slow process in the top level, thus alternating between the two stable states. It is conceivable that a third process in the full cascade could interact with an already oscillating two-layer system and thereby cause chaotic behavior.

An important question is whether oscillatory dynamics in the MAPK cascade play a role *in vivo*. Based on the early modeling results, it is often assumed that the cascade is utilized as an ultrasensitive switch, and other dynamics appear only as nonfunctional byproducts. Our results illustrate that the oscillatory parameter space is quite large and therefore likely to be encountered *in vivo*. This view is supported by the recent experimental observation of MAPK oscillations (Hilioti et al., 2008; Shankaran et al., 2009).

Further support for the functional role of oscillations comes from an evolutionary argument. If oscillations were indeed non-functional one could suspect that specific mechanisms suppressing oscillations should have evolved. Yet, the basic topology of the MAPK cascade that can sustain oscillations is conserved through evolution. By contrast, external feedback loops, that could potentially suppress oscillations, differ among organisms and cell types. Moreover, the two examples of feedback loops studied here were found to promote oscillations instead of suppressing them. If the MAPK cascade is indeed used both as a switch and as an oscillator under different physiological conditions, it is intuitive that the system should be very well conserved, as any further mutations are unlikely to maintain both of the cascade's function.

To ascribe biological function also to the irregular oscillations reported here is highly speculative. Nevertheless, it is conceivable that the observed spike-like dynamics could play a useful role. One could alternatively suspect that the complex oscillations are a byproduct of a mechanism that enhances differences between individual cells.

Such a mechanism may be useful because if in a population of cells, a substantial fraction of the populations changed their behavior at a similar level of an external stimulus, then the response would become switch-like also on the population level. This could have detrimental consequences because it could seriously decrease the dynamical stability on the population level and produce unnecessarily strong responses. It may therefore be advantageous to sustain a high sensitivity not only to the stimulus but also to enzyme concentrations that may differ between individual cells. Thereby, signals in different cells could be triggered at different levels of the stimulus, so that the response of the population is smooth, while the response of the individual cell stays sharp. Weakly chaotic dynamics could possibly arise as a byproduct of this internal sensitivity.

The question whether the detected forms of dynamics can appear *in vivo* is closely connected to the ques-

tion how realistic the space of parameters assessed in our study is. The ranges that we assigned to the general parameters were motivated by experimental data. While the total concentrations of the involved enzymes have been measured in one cell type (Huang and Ferrell, 1996), less is known about the remaining parameters. Note, however, that large differences in the fluxes f_i (see supplementary material) are to be expected since also the total concentration listed in Table 5 vary strongly between different layers. Therefore the parameter ranges in which oscillations and complex dynamics were observed in this study are not unreasonable. Nevertheless, future experimental work covering further variables and different cell types and developmental stages would be highly desirable to clarify the dynamics and function of the MAPK cascade *in vivo*.

5. Acknowledgments

The authors would like to thank Mark Fricker for insightful discussion of the results, especially regarding the potentially beneficial effects of weak chaos.

Appendix

Construction of the Jacobian

We demonstrate the construction of the Jacobian for the one-layer system, consisting of two phosphorylation steps. In a general form, the associated system of ODEs is

$$\begin{aligned}
\frac{\mathrm{d}}{\mathrm{dt}}S_1^1 &= f_9(S_3^1) - f_{10}(S_1^1, P_\mathrm{R}^1) + f_{11}(S_4^1) \\
&- f_{13}(S_1^1, K_\mathrm{R}^1) + f_{14}(S_5^1) + f_{18}(S_6^1) \\
\frac{\mathrm{d}}{\mathrm{dt}}S_2^1 &= f_{15}(S_5^1) - f_{16}(S_2^1, P_\mathrm{R}^1) + f_{17}(S_6^1) \\
\frac{\mathrm{d}}{\mathrm{dt}}S_3^1 &= f_7(S_0^1, K_\mathrm{R}^1) - f_8(S_3^1) - f_9(S_3^1) \\
\frac{\mathrm{d}}{\mathrm{dt}}S_4^1 &= f_{10}(S_1^1, P_\mathrm{R}^1) - f_{11}(S_4^1) - f_{12}(S_4^1) \\
\frac{\mathrm{d}}{\mathrm{dt}}S_5^1 &= f_{13}(S_1^1, K_\mathrm{R}^1) - f_{14}(S_5^1) - f_{15}(S_5^1) \\
\frac{\mathrm{d}}{\mathrm{dt}}S_6^1 &= f_{16}(S_2^1, P_\mathrm{R}^1) - f_{17}(S_6^1) - f_{18}(S_6^1)
\end{aligned}$$

From these equations, the stoichiometric matrix $\mathbf{N}$ is constructed according to the rule that $N_{i,j} = 1$ if f_{j+6} appears in the equation for S_i^1 with a positive sign, $N_{ij} = -1$ if f_{j+6} appears in the equation with a negative sign and $N_{ij} = 0$ else. Note that we use f_{j+6} for the sake of a consistent notation. Since the first layer of the cascade is not included in this model, the fluxes start with f_7 here.

Next, $\Lambda_{ij} = N_{ij} f_{j+6}/S_i^1$ is constructed from the stoichiometric matrix.

Assuming mass action, the matrix of derivatives is given by

$$\boldsymbol{\theta} = \begin{pmatrix}
-\frac{S_1^1}{S_0^1} & -\frac{S_2^1}{S_0^1} & -\frac{S_3^1}{S_0^1} - \frac{S_3^1}{K_\mathrm{R}^1} & -\frac{S_4^1}{S_0^1} & -\frac{S_5^1}{S_0^1} - \frac{S_5^1}{K_\mathrm{R}^1} & -\frac{S_6^1}{S_0^1} \\
0 & 0 & 1 & 0 & 0 & 0 \\
0 & 0 & 1 & 0 & 0 & 0 \\
1 & 0 & 0 & -\frac{S_4^1}{P_R^1} & 0 & -\frac{S_6^1}{P_R^1} \\
0 & 0 & 0 & 1 & 0 & 0 \\
0 & 0 & 0 & 1 & 0 & 0 \\
1 & 0 & -\frac{S_3^1}{K_\mathrm{R}^1} & 0 & -\frac{S_5^1}{K_\mathrm{R}^1} & 0 \\
0 & 0 & 0 & 0 & 1 & 0 \\
0 & 0 & 0 & 0 & 1 & 0 \\
0 & 1 & 0 & -\frac{S_4^1}{P_R^1} & 0 & -\frac{S_6^1}{P_R^1} \\
0 & 0 & 0 & 0 & 0 & 1 \\
0 & 0 & 0 & 0 & 0 & 1
\end{pmatrix}$$

The entries of $\boldsymbol{\theta}$ that are equal to 1 indicate linear dependencies.

The remaining nonzero entries arise due to indirect effects because of mass conservation. Here we show the calculation for

$$\theta_{x_1}^{\mu_1} = \left.\frac{\partial \mu_1}{\partial x_1}\right|_{\mathbf{S}=\mathbf{S}^*} \tag{7}$$

Assuming mass action, $f_7 = \alpha_7 S_0^1 K_\mathrm{R}^1$ with a rate constant α_7. It follows that

$$\theta_{x_1}^{\mu_1} = \frac{f_7}{f_7^*} = \frac{S_0^1 K_\mathrm{R}^1}{S_0^{1,*} K_\mathrm{R}^{1,*}} \tag{8}$$

Because of mass conservation of the substrate and the kinase, $S_0^1 = S_T^1 - S_1^1 - S_2^1 - S_3^1 - S_4^1 - S_5^1 - S_6^1$ and $K_R^1 = K_T^1 - S_3^1 - S_5^1$. Therefore, taking the derivative with respect to $x_1 = S_1^1/S_1^{1,*}$ gives

$$\theta_{x_1}^{\mu_1} = \left.\frac{\partial \mu_1}{\partial x_1}\right|_{\mathbf{S}=\mathbf{S}^*} = \frac{S_1^{1,*}}{S_0^{1,*} K_R^{1,*}} \left.\frac{\partial K_R^1 S_0^1}{\partial S_1^1}\right|_{\mathbf{S}=\mathbf{S}^*} = -\frac{S_1^{1,*}}{S_0^{1,*}} \tag{9}$$

The Jacobian $\mathbf{J} = \boldsymbol{\Lambda}\boldsymbol{\theta}_\mathbf{x}^{\boldsymbol{\mu}}$ can then be obtained by matrix multiplication. The resulting matrix is shown in the supplementary material.

Parameter Ranges

In the two-layer and the three-layer model we use parameters inferred from biologically reasonable ranges.

Parameter	Value
S_T^0	$2nM$
S_T^1	$1.2\mu M$
S_T^2	$1.2\mu M$
K_T^0	$0.3nM$
P_T^0	$0.3nM$
P_T^1	$0.3nM$
P_T^2	$120nM$

We choose the parameters based on data from *Xenopus* oocyte extracts (Huang and Ferrell, 1996).

We vary all total concentrations parameters by factors of 5 in the random sampling. The steady-state concentrations of all dynamic variables are then determined by the algorithm outlined in the main part of the paper.

Since we do not know of experimental data for typical steady-state fluxes $\mathbf{f}$, we tried to infer ranges for these quantities using information on rate constants. For each steady-state flux f_i, there is a rate constant α_i of the conventional model. From (Qiao et al., 2007) we adopt ranges of $30 - 750\text{min}^{-1}$ for α_{3n+2} and α_{3n} with $n = 1 \ldots 10$. Combining this with the steady-state concentrations, we can assign ranges to most fluxes. The remaining fluxes are determined by the flux modes. For this reason, and also because continuation of the generalized parameters in the bifurcation analysis alters also the parameters of the conventional models, we cannot guarantee that all α_i of conventional models remain restricted to these ranges. The α_i of the samples for which we show simulations are given in the supplementary material.

References

Blüthgen, N., Bruggeman, F., Legewie, S., Herzel, H., Westerhoff, H., Kholodenko, B., 2006. Effects of sequestration on signal transduction cascades. FEBS Journal 273, 895–906.

Chang, L., Karin, M., 2001. Mammalian MAP kinase signalling cascades. Nature 410, 37–40.

Downward, J., 2003. Targeting RAS signalling pathways in cancer therapy. Nature Reviews Cancer 3 (1), 11–22.

Eblen, S., Slack-Davis, J., Tarcsafalvi, A., Parsons, J., Weber, M., Catling, A., 2004. Mitogen-activated protein kinase feedback phosphorylation regulates MEK1 complex formation and activation during cellular adhesion. Mol Cell Biol 24, 2308–2317.

Fell, D., 1992. Metabolic control analysis: a survey of its theoretical and experimental development. Biochem. J. 286, 313–330.

Frey, S., Millat, T., Hohmann, S., Wolkenhauer, O., 2008. How quantitative measures unravel design principles in multi-stage phosphorylation cascades. J. Theor. Biol. 254 (1), 27–36.

Gross, T., Feudel, U., 2006. Generalized models as an universal approach to the analysis of nonlinear dynamical systems. Phys. Rev. E 73, 016205–14.

Gross, T., Rudolf, L., Levin, S., Dieckmann, U., 2009. Generalized models reveal stabilizing factors in food webs. Science 325, 747–750.

Guckenheimer, J., Holmes, P., 1997. Nonlinear oscillations, dynamical systems, and bifurcations of vector fields, 3rd Edition. Springer, New York.

Hairer, E., Wanner, G., 1991. Solving ordinary differential equations II: Stiff and differential-algebraic problems. Springer, Berlin.

Hilioti, Z., Sabbagh, Jr, W., Paliwal, S., Bergmann, A., Goncalves, M., Bardwell, L., Levchenko, A., 2008. Oscillatory phosphorylation of yeast Fus3 MAP kinase controls periodic gene expression and morphogenesis. Curr. Biol. 18, 1700–1706.

Hornberg, J., Binder, B., Bruggeman, F., Schoeberl, B., Heinrich, R., Westerhoff, H., 2005. Control of MAPK signalling: from complexity to what really matters. Oncogene 24, 5533–5542.

Huang, C., Ferrell, Jr, J., 1996. Ultrasensitivity in the mitogen-activated protein kinase cascade. Proc. Natl. Acad. Sci. 93, 10078–10083.

Johnson, G., Lapadat, R., 2002. Mitogen-Activated Protein Kinase Pathways Mediated by ERK, JNK, and p38 Protein Kinases. Science 298, 1911–1912.

Kelley, C., 2003. Solving nonlinear equations with Newton's method. SIAM, Philadelphia.

Kholodenko, B., 2000. Negative feedback and ultrasensitivity can bring about oscillations in the mitogen-activated protein kinase cascades. Eur. J. Biochem. 267, 1583–1588.

Kholodenko, B., 2006. Cell signalling dynamics in time and space. Nat. Rev. Mol. Cell Biol. 7 (3), 165–176.

Kolch, W., Calder, M., Gilbert, D., 2005. When kinases meet mathematics: the systems biology of MAPK signalling. FEBS Lett. 579, 1891–1895.

Kuznetsov, Y., 1995. Elements of Applied Bifurcation Theory, 3rd Edition. Springer Verlag, New York.

Langlois, W., Sasaoka, T., Saltiel, A., Olefsky, J., 1995. Negative Feedback Regulation and Desensitization of Insulin- and Epidermal Growth Factor-stimulated p21ras Activation. J. Biol. Chem. 270, 25320–25323.

Legewie, S., Schoeberl, B., Blüthgen, N., Herzel, H., 2007. Competing docking interactions can bring about bistability in the MAPK cascade. Biophys. J. 93, 2279–2288.

Markevich, N., Hoek, J., Kholodenko, B., 2004. Signaling switches and bistability arising from multisite phosphorylation in protein kinase cascades. J. Cell Biol. 164, 353–359.

Ortega, F., Garcés, J., Mas, F., Kholodenko, B., Cascante, M., 2006. Bistability from double phosphorylation in signal transduction. Kinetic and structural requirements. FEBS J. 273, 3915–3926.

Qiao, L., Nachbar, R., Kevrekidis, I., Shvartsman, S., 2007. Bistability and oscillations in the Huang-Ferrell model of MAPK signaling. PLoS Comput Biol 3, 1819–1826.

Roberts, P., Der, C., 2007. Targeting the Raf-MEK-ERK mitogen-activated protein kinase cascade for the treatment of cancer. Oncogene 26 (22), 3291–3310.

Seger, R., Krebs, E., 1995. The MAPK signaling cascade. The FASEB Journal 9 (9), 726.

Shankaran, H., Ippolito, D., Chrisler, W., Resat, H., Bollinger, N., Opresko, L., Wiley, H., 2009. Rapid and sustained nuclear–cytoplasmic ERK oscillations induced by epidermal growth factor. Molecular Systems Biology 5 (1).

Steuer, R., Gross, T., Selbig, J., Blasius, B., 2006. Structural kinetic modeling of metabolic networks. Proc Natl Acad Sci 103, 11868–11874.

Steuer, R., Nesi, A., Fernie, A., Gross, T., Blasius, B., Selbig, J., 2007. From structure to dynamics of metabolic pathways: Application to the plant mitochondrial TCA cycle. Bioinformatics 23, 1378–1385.

Stiefs, D., Gross, T., Steuer, R., Feudel, U., 2008. Computation and visualization of bifurcation surfaces. Int. J. Bifurc. Chaos 18, 2191–2206.

Stiefs, D., Venturino, E., Feudel, U., 2009. Evidence of chaos in eco-epidemic models. Math Biosci Eng 6, 855–871.

Tyson, J., Chen, K., Novak, B., 2003. Sniffers, buzzers, toggles and blinkers: dynamics of regulatory and signaling pathways in the cell. Curr Opin Cell Biol 15 (2), 221–231.

Van Voorn, G., Stiefs, D., Gross, T., Kooi, B., Feudel, U., Kooijman, S., 2008. Stabilization due to predator interference: comparison of different analysis approaches. Math. Biosci. Eng. 5, 567–583.

Ventura, A., Sepulchre, J., Merajver, S., 2008. A hidden feedback in signaling cascades is revealed. PLoS Comput Biol 4, 1–14.